PNAS RESEARCH ARTICLE | BIOPHYSICS AND COMPUTATIONAL BIOLOGY

Correlating histone acetylation with nucleosome core particle dynamics and function

Tae Hun Kim[a,b,c,d,1,2,3], Michael L. Nosella[b,d,2], Nicolas Bolik-Coulon[a,b,c], Robert W. Harkness[a,b,c,d], Shuya Kate Huang[a,b,c,d], and Lewis E. Kay[a,b,c,d,1]

Edited by Karolin Luger, University of Colorado Boulder, Boulder, CO; received January 18, 2023; accepted March 6, 2023

Epigenetic modifications of chromatin play a critical role in regulating the fidelity of the genetic code and in controlling the translation of genetic information into the protein components of the cell. One key posttranslational modification is acetylation of histone lysine residues. Molecular dynamics simulations, and to a smaller extent experiment, have established that lysine acetylation increases the dynamics of histone tails. However, a systematic, atomic resolution experimental investigation of how this epigenetic mark, focusing on one histone at a time, influences the structural dynamics of the nucleosome beyond the tails, and how this translates into accessibility of protein factors such as ligases and nucleases, has yet to be performed. Herein, using NMR spectroscopy of nucleosome core particles (NCPs), we evaluate the effects of acetylation of each histone on tail and core dynamics. We show that for histones H2B, H3, and H4, the histone core particle dynamics are little changed, even though the tails have increased amplitude motions. In contrast, significant increases to H2A dynamics are observed upon acetylation of this histone, with the docking domain and L1 loop particularly affected, correlating with increased susceptibility of NCPs to nuclease digestion and more robust ligation of nicked DNA. Dynamic light scattering experiments establish that acetylation decreases inter-NCP interactions in a histone-dependent manner and facilitates the development of a thermodynamic model for NCP stacking. Our data show that different acetylation patterns result in nuanced changes to NCP dynamics, modulating interactions with other protein factors, and ultimately controlling biological output.

nucleosome structural dynamics | methyl-TROSY NMR | conformational heterogeneity | nucleosomal DNA ligation and degradation

Significance

The fundamental repeating unit of chromatin is the nucleosome core particle (NCP), comprising two copies each of four different histones. Histone modifications play an important role in controlling chromatin structure and in maintaining the fidelity of DNA. Using a number of biophysical methods as well as biochemical assays, the effects of one type of histone modification, acetylation, on NCP structural dynamics are explored, correlating increased levels of dynamics in the NCP core with susceptibility to nuclease digestion and DNA repair. The role of acetylation in inter-NCP interactions is also studied, showing that histone acetylation modulates NCP stacking. Our studies demonstrate that acetylation can have a significant effect on the physical chemical properties of NCPs, regulating function.

Epigenetic modifications of chromatin regulate key cellular processes such as transcription (1, 2) and DNA damage repair (3, 4), and play essential roles in controlling cell differentiation and maintaining genome stability (5, 6). From a clinical point of view, epigenetic modifications are also closely linked to diseases such as cancer, diabetes, and neurological disorders (7–9). Enzymes often referred to as "writers" posttranslationally modify histones, which are the principal protein components of nucleosomes. The resulting modifications include, among others, acetylation, methylation, phosphorylation, ADP-ribosylation, and ubiquitination (1, 10). Histones modified in this manner are, in turn, recognized by "readers" that regulate the reorganization of chromatin structure in ways that depend on the type and location of the posttranslational modifications (PTMs), resulting in different biological effects on gene expression and the DNA damage response (11–13). This process is reversed by "erasers" which remove PTMs from histones.

One of the most well-characterized epigenetic marks is acetylation (14). Histone acetyltransferases (HATs) transfer an acetyl group from acetyl-Coenzyme A (acetyl-CoA) to the ε-amino group of lysine side chains, neutralizing the positive charge of these residues. As the lysine-rich histone tails are positively charged and interact with the negatively charged nucleosomal DNA, acetylation weakens histone tail–DNA interactions (1, 7). In terms of cellular function, histone acetylation is closely linked to transcription as it causes chromatin to transition from tightly packed (heterochromatin) to loosely packed (euchromatin) states (15, 16), rendering DNA more accessible to RNA polymerase II, transcription factors, and other proteins involved in transcriptional initiation and elongation. The transcriptional coactivator p300 (also known as EP300) is a key HAT that regulates gene expression by acetylating histones in the enhancer regions of genes (17). All the four core histones are acetylated by p300 in vivo with stronger preferences for H3 and H4 (18, 19). Dysregulation of p300 is associated with cancer by altering the expression of several oncoproteins and tumor suppressor proteins (20–22).

There is increasing evidence that histone acetylation is also involved in DNA damage repair pathways (12, 23–25). As chromatin structure regulates the accessibility of DNA to a variety of different factors, acetylation may facilitate DNA damage repair by controlling the interactions of DNA damage response/repair proteins with chromatin. In the

Author contributions: T.H.K., M.L.N., and L.E.K. designed research; T.H.K., M.L.N., N.B.-C., R.W.H., S.K.H., and L.E.K. performed research; T.H.K., M.L.N., and L.E.K. contributed new reagents/analytic tools; T.H.K., M.L.N., N.B.-C., R.W.H., S.K.H., and L.E.K. analyzed data; and T.H.K., M.L.N., and L.E.K. wrote the paper.

The authors declare no competing interest.

This article is a PNAS Direct Submission.

Copyright © 2023 the Author(s). Published by PNAS. This article is distributed under Creative Commons Attribution-NonCommercial-NoDerivatives License 4.0 (CC BY-NC-ND).

[1]To whom correspondence may be addressed. Email: txk560@case.edu or kay@pound.med.utoronto.ca.

[2]T.H.K. and M.L.N. contributed equally to this work.

[3]Present address: Department of Biochemistry, School of Medicine, Case Western Reserve University, Cleveland, OH 44106.

This article contains supporting information online at https://www.pnas.org/lookup/suppl/doi:10.1073/pnas.2301063120/-/DCSupplemental.

Published April 3, 2023.

case of base-excision repair, acetylation of K18 of histone 3 (H3K18) and H3K27 modulates the activity of the DNA repair enzymes UDG and APE1 (26), respectively, while acetylation of H4K16 facilitates homologous recombination-mediated double-strand break repair (27). In addition, acetylation of H3 and H4 by p300 has been shown to facilitate the recruitment of nonhomologous end joining proteins such as Ku70/80 to DNA damage sites (28).

Despite the importance of acetylation in regulating essential cellular processes and disease states, a detailed atomic resolution understanding of how it affects nucleosome structural dynamics remains elusive. This is partly because it is challenging to study intrinsically disordered regions of complexes, such as histone tails, which serve as focal points for acetylation (14, 29), using most standard biophysical tools. However, NMR spectroscopy offers unique advantages in this regard, and the availability of methyl-TROSY techniques for studying both protein (30, 31) and DNA (32) components of nucleosome particle core regions provides an opportunity for exploring how PTMs can affect nucleosome plasticity and ultimately function. Previous NMR studies of nucleosomes have provided structural insights into the role of histone tails in modulating interactions between nucleosome core particles (NCPs) and other proteins. Solution-state NMR studies by Musselman and coworkers showed that the H3 tail–DNA interaction impedes the binding of the PHD finger of BPTF to the NCP by sequestering the tail from other ligands (33). Relatedly, Bai and coworkers demonstrated that the K16Q mutation in H4, serving as a mimic for acetylation at this position, led to structural disorder of the basic patch region of the tail and to decreased compaction of nucleosomal arrays (34). Another solution-state NMR study established significant cross talk between H3 and H4 tails, whereby acetylation of the H4 tail enhances the dynamics of the H3 tail, leading to its increased acetylation rate (35). Stützer et al. have shown via solution NMR studies of NCPs that linker histones attenuate H3 tail dynamics, while PTMs of H3 tails that decrease positive charge led to an increase in dynamics, and subsequently, stronger interactions between the tail and other proteins (36). A recent solid-state NMR study led by Jaroniec focusing on H3 tails in nucleosome arrays has revealed that their dynamics are significantly decreased relative to what is observed in mononucleosomes, the result of interactions with linker DNA (37).

Further insights into the role of tail dynamics in regulating NCP stability, DNA sliding, and DNA unwrapping have been provided by molecular dynamics simulations, with tail truncations destabilizing the nucleosome and leading to increases in transient unwrapping of nucleosomal DNA (38). Modification of histone tails with charge-changing PTMs (such as acetylation or phosphorylation) or mutations was shown to significantly weaken histone tail–DNA interactions, while changes that preserve the tail charge states, such as methylation, did not result in such effects (39).

Recognizing the impact of acetylation on chromatin function, herein we systematically evaluate how this PTM modifies nucleosome structural dynamics by considering acetylation of each histone separately or several together, focusing on a single NCP. We make use of a strategy whereby a high level of acetylation is achieved on a given histone, subject to the constraint that intact and well-formed NCP particles are produced. Although this approach does not preserve the acetylation patters observed in vivo, it does ensure that perturbations to multiple lysine sites can be studied simultaneously, allowing the discovery of nuanced effects that might not otherwise be observed. This provides a foundation for additional studies focusing on particular lysines of interest. Using this acetylation scheme, we are able to assess whether there are similar changes to tail dynamics for each modified histone and whether such changes affect the mobility of the NCP core region, over the large range of time scales that can be probed by solution NMR (40, 41). Further, we investigate whether changes in dynamics correlate with changes in function through measurement of nucleosomal DNA accessibility to nucleases and ligases, and whether acetylation at sites in a particular histone might lead to more pronounced effects. Our NMR experiments establish that while acetylation of any of the four histones results in significant increases in the amplitude of pico (ps) – nanosecond (ns) timescale motions of the acetylated tail, for H2B, H3, and H4 there appears to be little accompanying change to the structural dynamics of the core region. In contrast, we observed significant increases in micro (μs) – millisecond (ms) timescale dynamics of histone H2A upon acetylation, in particular in the docking domain that contacts H3, and proximal to the L1 loop that stabilizes contacts between H2A molecules. Additionally, changes at the level of rapid timescale ps-ns motions were observed in these regions. Acetylation of H2A led to significant increases in DNA accessibility to nucleases and ligases relative to NCPs reconstituted with one of acetylated H2B, H3, or H4, with increased enhancements noted when H2A and at least one other histone in an NCP were acetylated, suggesting that acetylation can have a synergistic effect. Dynamic light scattering studies further establish that, consistent with decreased chromatin compaction upon acetylation (42), histone acetylation, particularly of H4, reduces inter-NCP interactions. Our study thus paints a picture of how different acetylation patterns can result in nuanced and very significant changes to NCP dynamics and interactions, thereby regulating access of key proteins to nucleosomal DNA and ultimately modulating function.

Results

Preparation of Acetylated NCPs. Here, we have used the smallest building blocks of chromatin, NCPs, comprising two copies each of histones H2A, H2B, H3, and H4, wrapped with 153-base pair Widom 601 DNA (43), to study the effects of acetylation on histone dynamics. The relatively small size of NCPs (~210 kDa), compared to chromatin, makes these particles amenable to detailed studies by solution NMR, where the highly flexible tails can be probed using ^{15}N-based experiments, as has been done previously (33, 34, 44), and the core dynamics assessed through methyl-TROSY approaches focusing on $^{13}CH_3$ groups (30, 31). Samples were generated where the histone of interest was either uniformly ^{2}H,^{13}C,^{15}N labeled (^{15}N relaxation and backbone assignments), or labeled with $^{13}CH_3$ methyl groups at Ile(δ1), Leu, and Val positions (only one of the two isopropyl methyl groups of Leu/Val was labeled nonstereospecifically (45); referred to in what follows as ILV-labeling). The remaining three histones were highly deuterated, but not isotopically enriched in either ^{15}N or ^{13}C, rendering them invisible in the NMR experiments performed.

NCPs with different acetylation patterns were prepared by first incubating each histone (separately) with the catalytic domain of the transcriptional coactivator p300 in the presence of acetyl-CoA (Fig. 1*A*). After validating the number of acetyl groups on the histones by mass spectrometry and removing p300, H2A-H2B dimers and H3-H4 tetramers were reconstituted with different combinations of acetylated and unmodified histones, depending on the experiment. Variably acetylated dimers and tetramers were wrapped with 601 DNA, and the homogeneity and integrity of the resulting NCPs were validated by native gel electrophoresis (Fig. 1*A*; acetylation decreases the electrophoretic mobility of the NCPs on a native gel). Histone acetylation did not generally

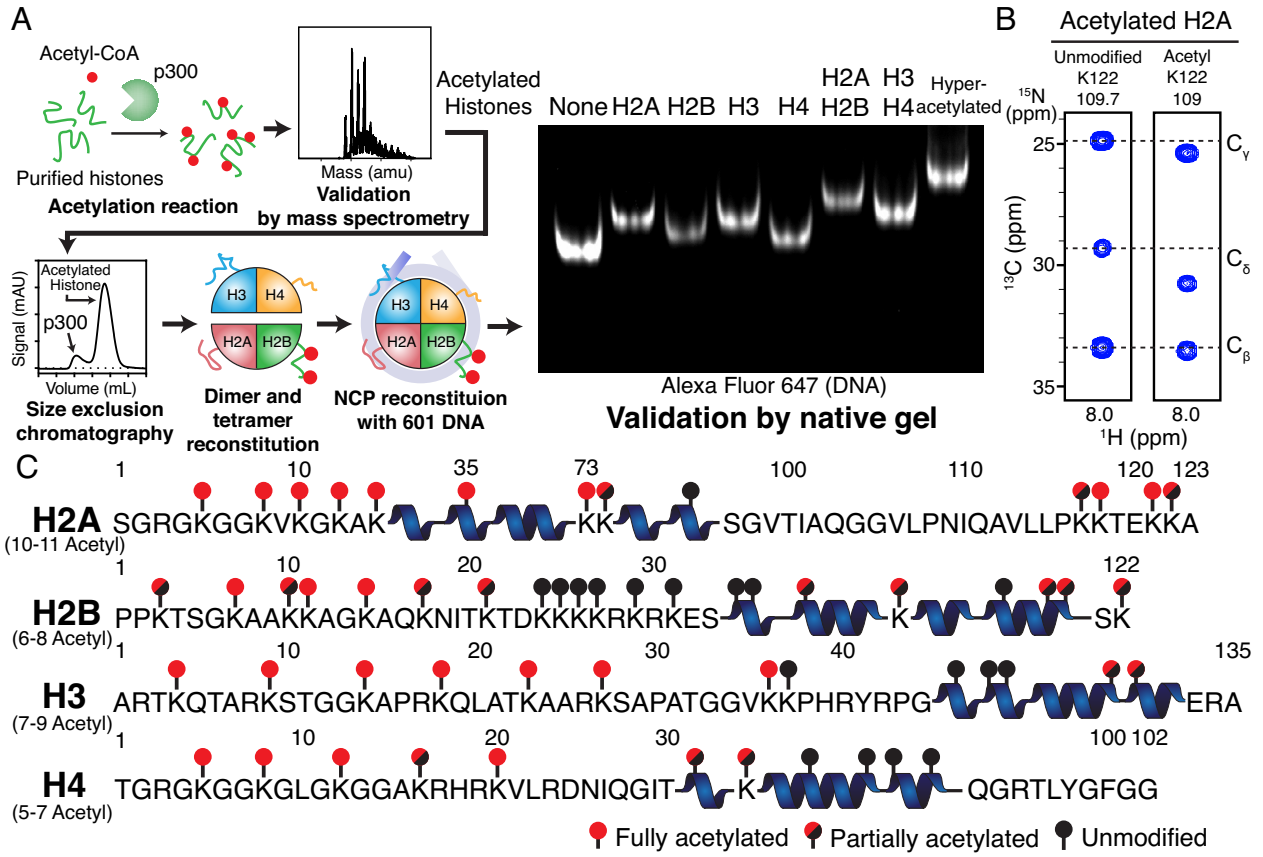

Fig. 1. Preparation of acetylated NCPs and locations of acetyl groups in histones. (*A*) General scheme for preparing NCPs with different acetylation patterns. After reconstitution is complete, sample integrity is verified by native gel electrophoresis (*Right*), showing NCP samples without acetylation (None), or acetylation at one or more sites (for example, H2A denotes acetylation of H2A only, hyperacetylated is acetylation of all the four histones). Gel mobility decreases with increasing acetylation. (*B*) ^{1}H–^{13}C 2D strips for K122 of acetylated H2A, dissolved in 6 M urea, from a 3D C(CO)NH spectrum (46) (25 °C, 18.8 T) showing changes in ^{13}C chemical shifts of unmodified (*Left*) and acetylated (*Right*) K122 sidechains. From the ratio of peak intensities in the corresponding ^{1}H–^{15}N dataset or from intensities of sidechain peaks in the C(CO)NH spectrum, it is possible to quantify the fraction that is modified. For example, the K122 modification is clearly incomplete, as two sets of peaks are visible for this residue. (*C*) Schematic view of histone primary sequences identifying acetylation sites and the degrees of modification at each position. Average ranges of acetylation are noted below each histone. Red circles denote lysine residues that are fully acetylated, while black and half-red-half-black circles denote unmodified and partially acetylated lysine residues, respectively.

compromise the homogeneity of the NCPs, except in the case of H2B, for which maximal acetylation caused multiple species to emerge in the native gel analysis. We suspect that a high level of H2B acetylation (11 to 12 sites) disrupts interactions within the histone octamer, thereby preventing the proper formation of the NCP. We therefore limited the number of acetylated sites to eight for H2B, as this level of modification did not affect the homogeneity of the NCPs, by using an eight-molar excess of acetyl-CoA relative to H2B, rather than the 20-fold excess used for the remaining histones.

Identification and Quantification of the Acetyl-Lysine Residues in Histones. In order to identify the sites of acetylation and the extent of modification at each lysine site, we used a suite of triple-resonance NMR experiments to first assign the amide chemical shifts of each acetylated ^{13}C,^{15}N-labeled histone in denaturing 6 M urea buffer. As in a standard assignment procedure involving a homogeneous sample, connectivities were propagated from one residue to the next (47). In some cases, close to a Lys residue, the assignments diverged into separate paths that then reconverged, reflecting heterogeneity in acetylation of an intervening Lys. With the backbone assignments available, Lys sidechain ^{13}C chemical shifts were obtained, reporting directly on the acetylation status of each Lys position. Fig. 1*B* shows a pair of strips from a C(CO)NH spectrum (46) of acetylated H2A focusing on K122. As acetylation gives rise to marked perturbations of Lys sidechain ^{13}C chemical shifts (48), it is straightforward to assign chemical shifts for the acetylated and unmodified forms of each lysine residue, and hence obtain the fraction of labeling at a given lysine position from amide peak intensities (*SI Appendix*, Fig. S1). On average, 5 to 9 lysine residues of H2B, H3, and H4 were acetylated while a higher number (10 to 11 sites) of modifications was observed for H2A (Fig. 1*C*). The numbers of acetyl groups for each histone calculated based on the NMR analysis closely matched those determined by mass spectrometry (*SI Appendix*, Fig. S2), with the NMR approach described above providing a facile way for quantifying the extent of the modifications at each site.

Acetylation Enhances Histone Tail Dynamics. Fig. 1*C* shows that most of the acetylated lysines are located in the histone tails, which generally extend out of the core particle (Fig. 2*A*). Not surprisingly, therefore, these often long, protruding tails have a much higher degree of flexibility than the remainder of the histone polypeptide chains, facilitating the use of standard backbone ^{15}N-based experiments, both for resonance assignments and subsequent spin relaxation studies to address how acetylation specifically affects histone tail motions. Fig. 2*B* overlays amide spectra of unmodified and acetylated ^{2}H,^{13}C,^{15}N-labeled H3 NCPs (37 °C, 18.8 T; all other histones are perdeuterated), illustrating the high quality of data that are available from the tail regions of the complex.

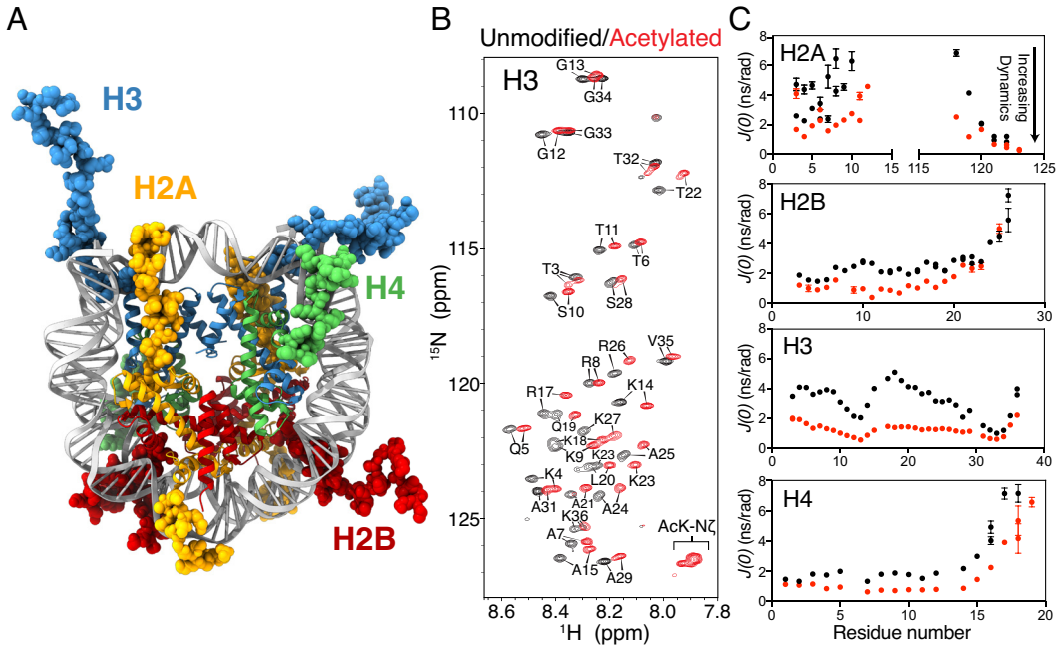

Fig. 2. Backbone histone tail dynamics are enhanced by acetylation. (*A*) Structure (PDB ID: 1KX5) of the NCP highlighting the position of each histone tail. Colors denote histone H2A (yellow), H2B (red), H3 (blue), and H4 (green). (*B*) Overlaid amide HSQC spectra of unmodified (black) and acetylated (red) ^{2}H,^{13}C,^{15}N-labeled H3, ^{2}H-{H2A, H2B, H4} NCPs (37 °C, 18.8 T). Note that only residues from the tail region of H3 could be observed, despite ^{15}N labeling at all nitrogen sites. (*C*) Plots of *J*(0) values of unmodified (black) and acetylated (red) histone tails of each of the four histones, 37 °C.

Although deuteration is not necessary to observe the majority of crosspeaks from the tail residues, both in the case of H3 and for the other histones as well, there are significant improvements in signal-to-noise ratios for correlations that derive from regions of the tails closest to the structured core of the NCP in the case where deuteration is used. Notably, crosspeaks were not present in ^{1}H–^{15}N spectra for amides in the core of the complex, even for deuterated particles, because of the large size of the NCP, as has been noted before (44, 49). Larger chemical shift perturbations (CSPs) were observed for backbone amides of the acetylated lysine residues, with peaks from neighboring residues experiencing modest CSPs upon acetylation (*SI Appendix*, Fig. S3).

In order to probe the amplitudes of histone tail motions properly, it is necessary to separate contributions to transverse relaxation from motions on different timescales. This can be achieved by recording a series of ^{1}H–^{15}N relaxation experiments from which the obtained rates are combined to yield exchange-free measures of ^{15}N relaxation from dipole–dipole interactions exclusively (50). Fits of such datasets, along with ^{15}N R_1 and steady-state ^{1}H–^{15}N heteronuclear Overhauser effect (NOE) measurements, allow the extraction of per-residue *J*(0) values (50) that can be used as a simple metric to evaluate the "extent of motion" at a given amide, with increasing *J*(0) indicating less dynamics (*SI Appendix*, Measurement of Dynamics in NCPs). Fig. 2*C* plots *J*(0) values for each of the four histone tails (note that H2A has N- and C-terminal tails), both without (black) and with (red) acetylation. In all cases, tail modification leads to decreases in *J*(0) values, reflecting a higher degree of motional freedom for the acetylated tails than their unmodified counterparts. This result is consistent with previous observations that the electrostatically driven interactions between the Lys-rich histone tails and the nucleosomal DNA are weakened by acetylation (51, 52). It is noteworthy that relative to H2B and H4, larger increases in the extent of ps-ns timescale dynamics were observed for H2A and H3 tails upon acetylation. Perhaps not unexpectedly, therefore, unmodified H2A and H3 tails showed elevated *J*(0) values compared to unmodified H2B and H4, consistent with their engagement in more extensive interactions with nucleosomal DNA. Interestingly, the number of acetylated lysines in the N-terminal tail of H2A is not larger than that for H2B or H4 (approximately five in each case), and the lysine density (fraction of lysine residues in the tail) is comparable for H3, H2B, and H4, suggesting that the relation between increased tail dynamics and acetylation likely involves some interplay between both parameters (i.e., number and density), in addition to the relative position of the lysines in relation to the nucleosome DNA. However, it may be the case that more than two-fold increase in lysine density in the case of H2A (5 of 15 N-tail residues) does significantly contribute to the observed change in ps-ns timescale motions upon acetylation. Finally, it is also possible to combine the relaxation data that yield *J*(0) values above in a different way to estimate contributions from conformational exchange to the measured ^{15}N transverse relaxation rates (53). These are, however, very small for each of the four tails. In summary, our data establish that acetylation enhances the ps-ns dynamics of all the four histone tails, with the largest changes occurring in H2A and H3.

Increased NCP Core Dynamics upon Acetylation of H2A. Having established that all of the histone tails show significant increases in dynamics upon acetylation, we next asked how the NCP core would be affected by this modification. To this end, we used methyl-TROSY-based methods, as the backbone amides were not visible in the core region of the nucleosome particle. Four acetylated NCP samples, each comprised of a single acetylated, ILV-labeled histone (the remaining histones were deuterated), were prepared and analyzed by recording ^{1}H–^{13}C heteronuclear multiple quantum coherence (HMQC) spectra (37 °C, 23.5 T). Fig. 3*A* shows overlays of datasets recorded of unmodified (black) and acetylated (red) NCPs focusing on histones H2A (*Left*) and H3 (*Right*). Similar quality spectra were obtained with/without acetylation for H3, as well as for H2B, and H4 with only small CSPs primarily in the tail regions where acetylation

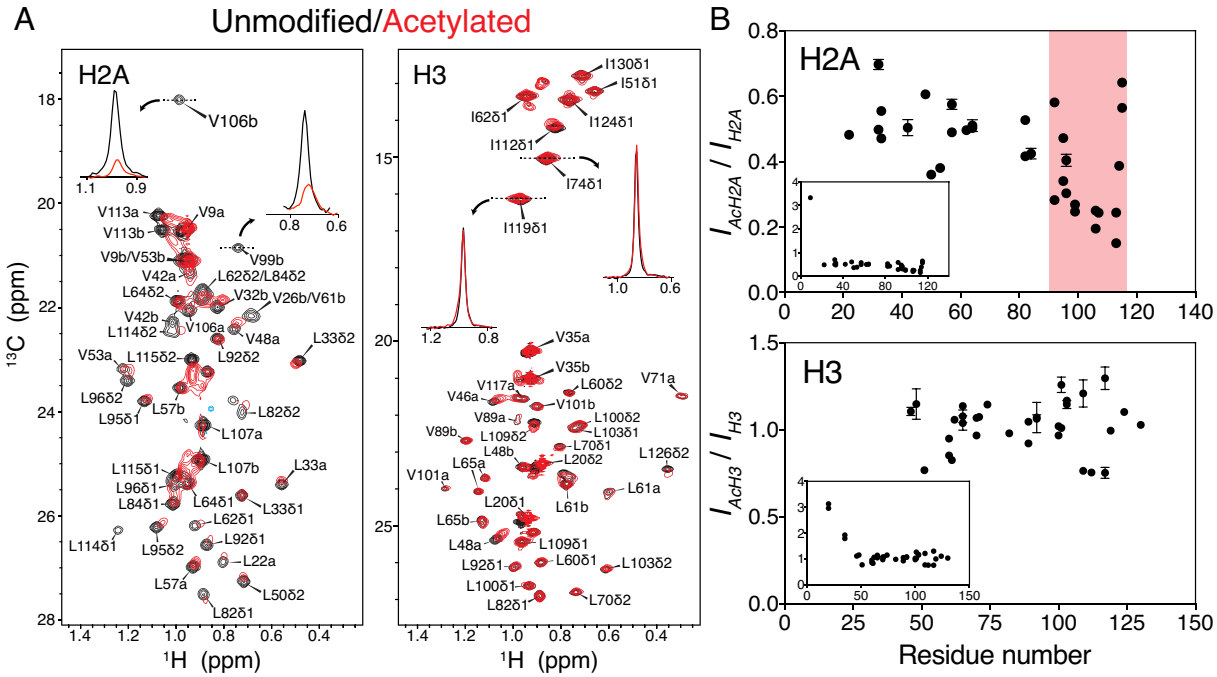

Fig. 3. Acetylation of H2A, but not other histones, leads to significant conformational heterogeneity. (*A*) Overlay of ^{1}H–^{13}C HMQC spectra of H2A- (*Left*; ILV-H2A) or H3- (*Right*; ILV-H3) unmodified (black) or acetylated (red) NCPs, recorded at 23.5 T, 37 °C. One-dimensional traces at the ^{13}C resonance frequencies of V106b and V99b highlight the changes in peak intensities upon acetylation. Stereospecific assignments for prochiral methyl groups of Leu and Val are indicated wherever they are available; otherwise, methyls are denoted by "a" or "b." (*B*) Methyl group peak intensity ratios (acetylated/unmodified; for example, I_{AcH2A}/I_{H2A} for ILV-labeled histone H2A in the NCP) plotted as a function of sequence. *Insets* show peak intensity ratios for all residues, including in the N-terminal tails where intensity ratios are greater than 0.8 (*Top*) or 1.5 (*Bottom*).

occurs (*SI Appendix*, Fig. S4*A*). Notably, methyl peak intensities in core regions remained relatively uniform for histones H2B, H3, and H4, consistent with little change in mobility upon acetylation, while methyl groups localized to the tails showed increased intensities (Fig. 3 *B*, *Bottom* and *SI Appendix*, Fig. S4*B*) upon acetylation, indicating increased dynamics, as expected from the ^{15}N data. In contrast, the quality of the H2A spectrum was significantly compromised by acetylation with significant peak broadening, more extensive peak shifts (Fig. 3 *A*, *Left*), and reduced intensities throughout, but especially focused on the C-terminal region extending from residues 92-114 (Fig. 3 *B*, *Top*). As with the other three histones, the N-terminal tail of H2A was more dynamic in the acetylated state, as evidenced by the threefold increase in the intensity of the correlation from V8 relative to the unmodified tail.

The extensive broadening of crosspeaks in HMQC spectra of acetylated H2A, especially for the methyl groups localized to the C-terminal region of the histone (Fig. 3 *B*, *Top*), is consistent with dynamics on the μs-ms timescale. In order to quantify this motion in a more rigorous manner, we recorded methyl-TROSY-based Carr–Purcell–Meiboom–Gill (CPMG) relaxation dispersion experiments (54) on both acetylated and unmodified ILV-labeled NCP samples (one histone labeled at a time) at both 14.1 T and 23.5 T. In this class of experiment, the effective transverse relaxation rates of multiple-quantum coherences ($R_{2,eff}$) are measured as a function of the number of chemical shift refocusing pulses, $R_{2,eff}$ vs. ν_{CPMG} [ν_{CPMG} = 1/(4δ), where 2δ is the time between successive pulses], and the resultant dispersion profiles fit to a model of chemical exchange. Flat profiles were observed for all histones within the unmodified NCPs, and for NCPs comprising one of the acetylated H2B, H3, and H4, indicating that μs-ms timescale motions could not be detected using methyl group probes in these molecules. However, acetylation of histone H2A led to measurable μs-ms timescale dynamics (red circles in Fig. 4*A*), as the profiles are not flat, a result expected from the relatively poor quality of the corresponding ^{1}H–^{13}C spectrum. A model of two-site chemical exchange was able to fit the dispersion profiles (Fig. 4*A* and *SI Appendix*, Fig. S5; black lines), yielding values of the exchange rate and population of a minor second state of 900 ± 100 s^{-1} and 14 ± 1%, respectively. Interestingly, significantly different $R_{2,eff}$ rates were observed at high ν_{CPMG} values in profiles derived from H2A methyl groups in acetylated and unmodified NCPs (for example, V42, L107, L115 in Fig. 4*A*). In the case of V42 and L107, the higher $R_{2,eff}$ rates at ν_{CPMG} = 1.2 kHz, where the dispersions have plateaued, suggest that in addition to motion within the ms window, acetylation introduces faster dynamics within the μs timeframe whose effects cannot be eliminated with the pulsing frequencies used. In the case of L115, the deviation observed, whereby acetylation lowers $R_{2,eff}$ values, reflects the fact that the interaction between the C-terminal tail residues and nucleosomal DNA is diminished by acetylation, giving rise to increased mobility and hence slower transverse relaxation. In general, both ps-ns motions and μs dynamics may be present and whether the plateau regions of the profiles derived from methyl groups within H2A-acetylated NCPs are above or below the corresponding plateau regions in curves from unmodified NCPs depends on the relative contributions of the dynamics from each of the motional regimes.

Many of the sites displaying increased μs-ms timescale dynamics are localized to the H2A docking domain, a region including residues 81 to 116 that plays an important role in stabilizing the NCP by making interactions with the neighboring histone H3 (Fig. 4 *B*, *Top Inset* and *Discussion*) (55), while V42 is within the L1 loop that forms L1–L1 loop contacts between adjacent H2A histones, thus further stabilizing the core structure (*Bottom Inset*) (55). It is noteworthy that some of the acetylation sites on H2B,

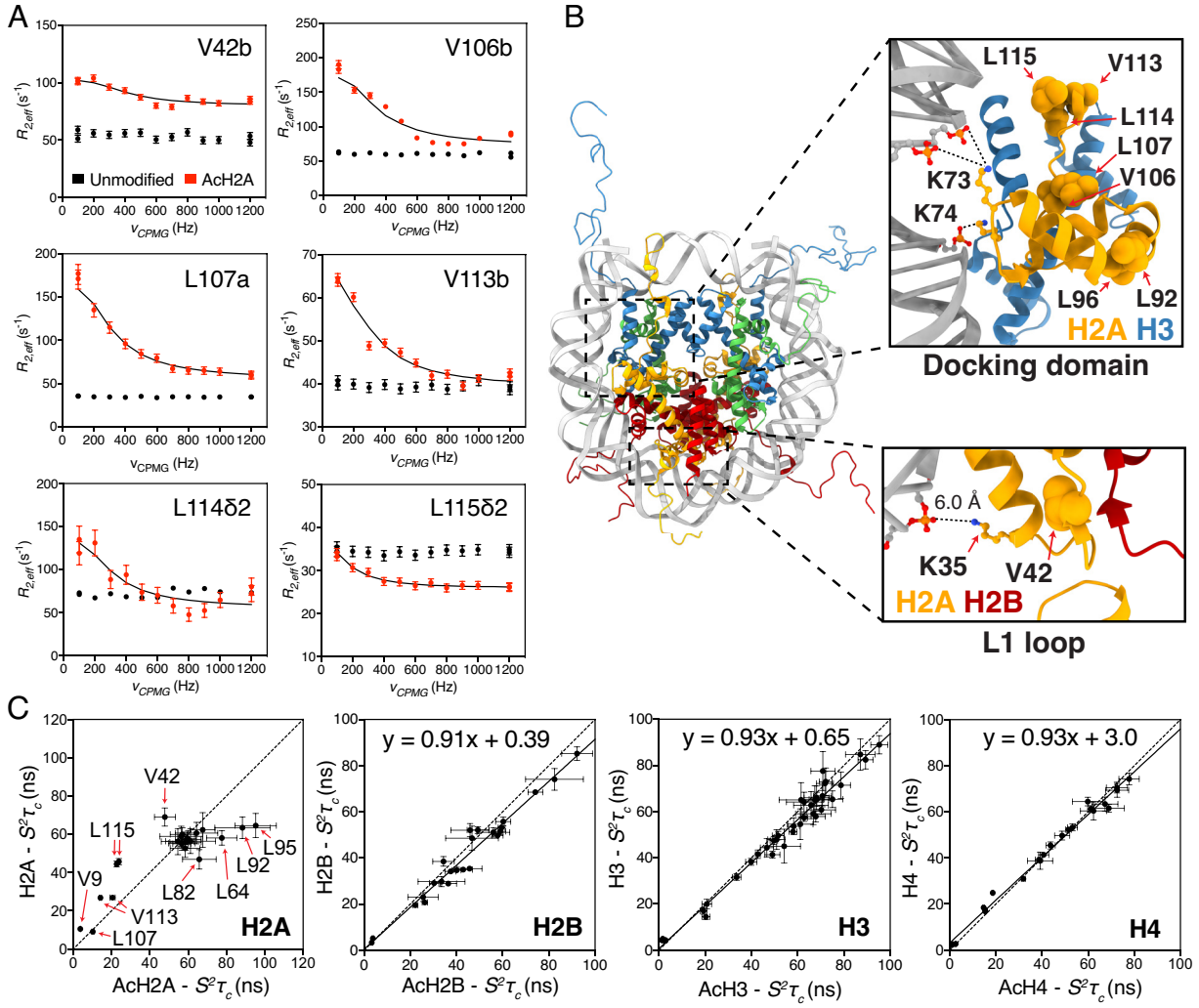

Fig. 4. H2A ps-ns and µs-ms dynamics are significantly affected by acetylation. (*A*) ^{1}H–^{13}C multiple-quantum CPMG relaxation dispersion profiles of unmodified- (black) and acetylated- (red) H2A-containing NCPs (only H2A is ILV labeled; other histones are perdeuterated), 23.5 T, 37 °C. Additional data recorded at 14.1 T, 37 °C, are shown in *SI Appendix*, Fig. S5. Best fits from a combined analysis of datasets recorded at both fields are shown as solid lines. (*B*, *Left*) Structure of the NCP [PDB ID: 1KX5], highlighting the docking domain (*Right*, *Top*) and the L1 loop (*Right*, *Bottom*) with the following color scheme, yellow (H2A), red (H2B), blue (H3), green (H4), and gray (DNA). Methyl groups with $R_{2,eff}$(100 Hz) − $R_{2,eff}$(2000 Hz) > 7 s^{-1} are indicated as spheres in the zoomed images. The electrostatic interactions between lysine residues (K35, K73, and K74) and the phosphate backbones of nucleosomal DNA are shown in the zoomed images. (*C*) Linear correlation plots of $S^2_{axis}\tau_C$ values of corresponding methyl groups in NCPs comprised of unmodified *vs* acetylated histones, as indicated. Dashed and solid lines correspond to y = x and best linear fits, respectively. Equations for solid lines are indicated in the panels. All data were recorded at 23.5 T, 37 °C, with the exception of data for H2A which were obtained at 14.1 T, 37 °C, to minimize contributions from µs-ms timescale dynamics. H2A residues with significant deviation from y = x are indicated with their residue numbers.

H3, and H4 are proximal to DNA (*SI Appendix*, Fig. S6), much like for H2A, yet modification of these did not lead to conformational heterogeneity of the core. Thus, whether significant effects on the structural dynamics of the NCP core region are observed must depend on the location of the modified sites in relation to the DNA, and on the nature of the histone–histone and histone–DNA interactions in the region of the perturbation.

Having established that acetylation of H2A leads to µs-ms timescale motions in key regions involved in interhistone contacts, we asked whether we could observe changes to dynamics in the ps-ns window. We, therefore, recorded experiments that are sensitive to intramethyl group ^{1}H–^{1}H relaxation from which site-specific values of $S^2_{axis}\tau_C$ could be obtained, where S_{axis} is the order parameter for the methyl three-fold axis, reflecting the amplitude of motions of the methyl group in question, and τ_C is a residue-specific effective correlation time for the overall rotation of the methyl (*SI Appendix*, Fig. S7). Strong correlations are observed between $S^2_{axis}\tau_C$ values for corresponding methyl groups in NCPs containing acetylated and nonacetylated H2B, H3, and H4 (Fig. 4*C*; solid lines), with the slight deviation from y = x (dashed line) likely reflecting the minor differences in overall tumbling times of the particles caused by the histone modifications, and, therefore, the subsequent changes in the interaction between the tails and the core particle. In contrast, the correlation is much worse for H2A (Fig. 4 *C*, *Left*), in particular for residues in the C-terminal portion of the docking domain (V113, L115), and in the L1 loop (V42) for which $S^2_{axis}\tau_C$ values decrease upon acetylation (increased motion) and for other residues in the docking domain that are more central (for example, L82, L92, L95) and which showed changes in slower timescale dynamics as well (Fig. 4*A* and *SI Appendix*, Fig. S5).

In order to test whether acetylation of the four C-terminal lysine residues in H2A (K117, K118, K121, and K122) – and hence the decrease in tail–DNA interactions – are responsible, at least partly, for the observed changes in core particle dynamics relative to unmodified H2A, we prepared an H2A mutant wherein a portion

of the C-terminal tail including all the four terminal lysine residues was deleted (eight residue deletion, referred to as P116*; the asterisk represents a stop codon). In this sample, interactions between the C-terminal tail and nucleosomal DNA are eliminated, as the lysines are missing, much like when the C-terminal lysines are acetylated, so that the absence of terminal lysine–DNA interactions on core dynamics can be readily assessed. Relaxation dispersion profiles (μs-ms timescale motions) and $S^2_{axis}\tau_C$ (ps-ns) values for an H2A P116* NCP sample (no acetylation) were measured. Notably, only flat CPMG profiles were obtained (*SI Appendix*, Fig. S8*A*), with some changes in ps-ns motions involving the C-terminal tail (for example, V99, V106, and L115) although not as extensive as before (*SI Appendix*, Fig. S8*B*). This suggests that a major contribution to the observed dynamics of acetylated H2A NCPs derives from acetylation at sites distinct from the C terminus. Indeed, extensive peak broadening, especially focused on the H2A docking domain, was present in the HMQC spectrum of a mutant H2A (K73Q, K74Q, P116*) NCP sample (*SI Appendix*, Fig. S9), where the lysine to glutamine substitutions at positions 73 and 74 are mimics of acetylation (34). In addition, the residues in the docking domain exhibited large CPMG dispersion profiles (*SI Appendix*, Fig. S8*B*). Very similar increases in dynamics were observed upon acetylation of H2A, as discussed above (Fig. 4*A*), establishing the importance of K73 and K74 in stabilizing the core particle (Fig. 4 *B*, *Top Inset*).

Effect of Acetylation on NCP–Enzyme Interactions. The regulation of enzymatic functions occurring on nucleosome-associated DNA can be controlled by the strength of the histone–DNA interactions (56, 57). We hypothesized, therefore, that the acetylation-dependent dynamical changes we observed by NMR, involving each of the histone tails, and the core region of H2A, might correlate with enhanced DNA-directed enzymatic activity in the context of the NCP. To test this hypothesis, and to further establish the relative effects of acetylation of different histones, we designed NCPs with a single-strand break-containing 601-DNA sequence to use in a DNA ligation assay (Fig. 5*A*). The 5′-phosphates were removed from the ends of the DNA to ensure that ligase activity was only localized to the nicked region (*SI Appendix*, *Materials and Methods*), and a fluorophore was attached on the 3′-end for easy visualization on urea-denaturing gels (Fig. 5*B*). DNA ligases must fully encircle duplex DNA in order to catalyze ligation, possibly explaining why some ligases, such as DNA ligase 3 (LIG3), exhibit diminished activity on nicked DNA substrates that are incorporated into nucleosomes (58, 59). Ligase activities were measured by quantifying the extent of repair over time via analysis of ligation gels (Fig. 5 *B* and *C* and *SI Appendix*, Fig. S10*A*) from which repair rates were calculated (Fig. 5*D* and *SI Appendix*, Fig. S10*B*). Under the conditions used in our assay, we observed low amounts of LIG3 activity on nicked 601-DNA in unmodified or acetylated H2B NCPs (Fig. 5*D*; see *Inset* of Fig. 5*D* for the position of the DNA nick), with slightly higher rates for NCPs containing acetylated H3 or H4. Notably, ligation increased dramatically when H2A was acetylated. Different combinations of acetylation on multiple histones caused varying effects, though generally the extent of ligation was greater than when any of the histones included in the combination were acetylated separately. In particular, acetylation of the H2A-H2B dimer caused a further increase in ligation beyond that measured for H2A acetylation alone (Fig. 5*D*), and more than would be expected if the effects were additive, suggesting that some level of cooperativity may emerge when multiple histones are acetylated simultaneously.

As H2A acetylation showed the strongest effect in our ligation assay, we were interested in exploring what modifications might be most responsible for the large increase in DNA repair. In order to investigate the role of acetylation at the four C-terminal lysine residues, we prepared nicked-601 DNA-containing NCPs with the P116* truncation (no acetylation) and observed only a small increase in the ligation rate (Fig. 5 *C* and *D*). As described above, the H2A C terminus contains a segment called the docking domain that strongly influences nucleosome stability and the extent of transient DNA unwrapping (55, 60), and several of the identified acetylation sites in H2A are adjacent to this region (Fig. 1*C*, K73 and K74). We therefore monitored ligation in a mutant H2A (K73Q, K74Q, P116*) NCP sample, noting a significant increase in repair rates (Fig. 5 *C* and *D*), although much less than observed for the acetylated H2A sample. It is likely, therefore, that a synergistic effect involving lysine modifications at both N- and C-terminal H2A tails, spanning the length of the nucleosome, as well as lysines that are in the core region, is required to achieve the high levels of ligation rates noted for acetylated H2A. However, we cannot rule out the possibility that the K to Q mutations do not fully recapitulate the effects of acytelation.

In order to validate the remarkably high repair rates noted for acetylated H2A NCPs, we employed a micrococcal nuclease (MNase) sensitivity assay to evaluate how the different histone acetylation patterns modulate accessibility of nucleosomal DNA. MNase is a sequence-nonspecific exo- and endonuclease which readily degrades exposed DNA — that is, DNA that is not engaged in protein interactions. The ability of nucleosomes to protect DNA from MNase digestion is well established (61, 62). We found that the 601-DNA contained in unacetylated NCPs was partially degraded by MNase within 5 min under the prescribed reaction conditions (*SI Appendix*, *Materials and Methods* and Fig. 5*E*). The extent of degradation was qualitatively similar for NCPs containing acetylated H2B, H3, or H4 but was substantially higher in the case of H2A acetylation. As in the ligation experiments, the extent of MNase digestion was further enhanced when multiple histones were acetylated simultaneously, with the greatest effects again emerging in combinations that included acetylated H2A.

Different Acetylation Patterns Disrupt Internucleosome Interactions to Various Degrees. The NMR spin relaxation experiments described above focus on intra-NCP interactions and how changing these by acetylation affects core particle dynamics, and ultimately the interaction of NCPs with other protein molecules such as those involved in DNA ligation and degradation. Yet, chromatin structure depends on interactions between nucleosomes (63) and it is well established that histone tails are crucial for internucleosome interactions (64), with contacts between the H4 tail and the H2A/H2B acidic patch known to be particularly important (65). We were interested, therefore, to see whether tail modifications through acetylation would regulate interactions between single nucleosome particles as well. We measured dynamic light scattering (DLS) and extracted z-average diffusion constants (D_z) of unmodified and acetylated NCPs across a range of NCP concentrations spanning 1 to 100 μM (Fig. 6*A*) in the presence of 100 mM sodium chloride and 20 mM sodium phosphate (and in the absence of sodium chloride, *SI Appendix*, Fig. S11*A*). Values of the effective hydrodynamic radii, R_h, of the particles (calculated using the Stokes–Einstein relation) as a function of NCP concentration are shown in Fig. 6*A*, with linear fits illustrated. The D_z vs. NCP concentration profiles (Fig. 6 *B*, *Left*) could be well fit using a self-assembly model (Fig. 6 *B*, *Right*, *Bottom* and *SI Appendix*, *Materials and Methods*), assuming that the association of neighboring NCPs occurs via a

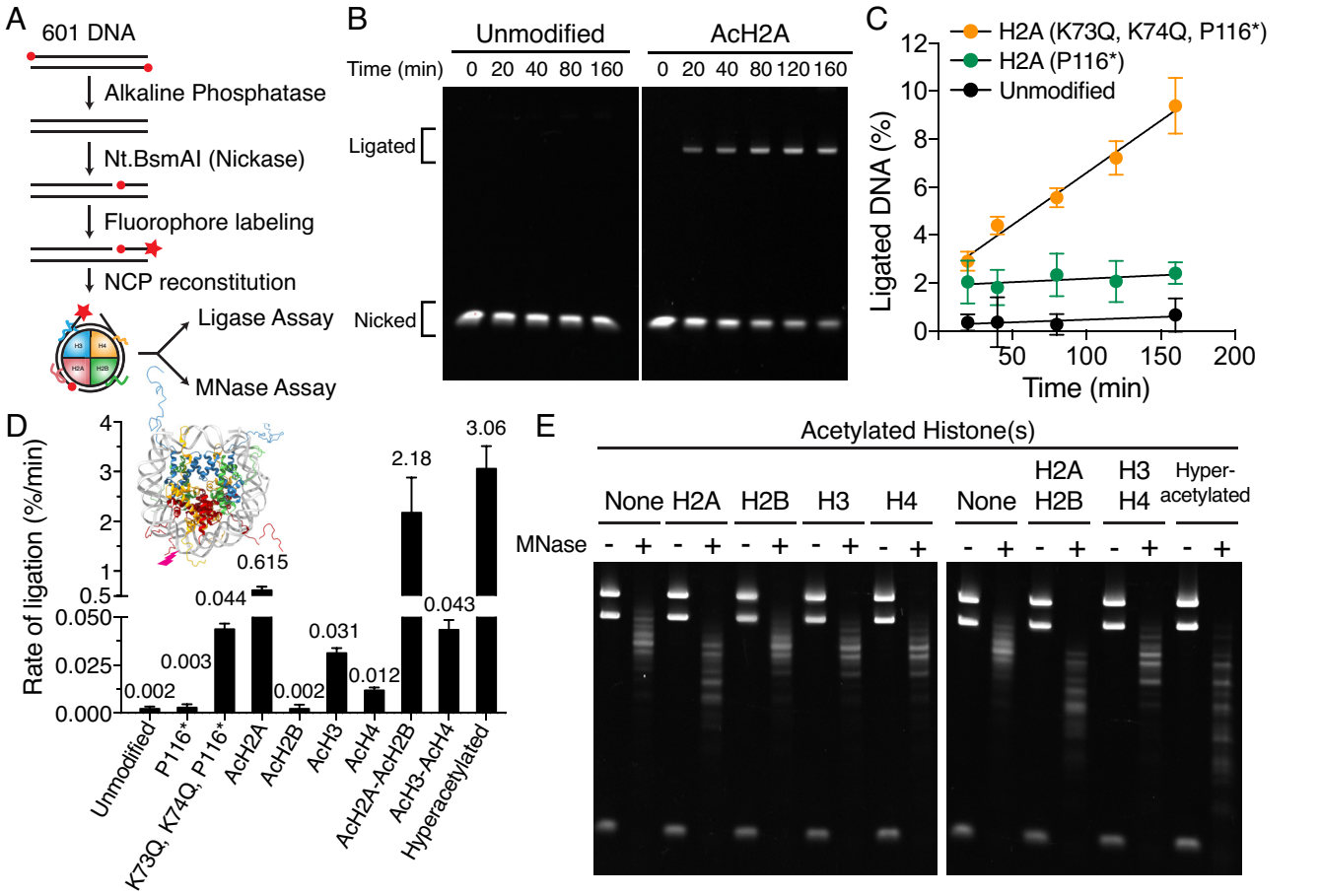

Fig. 5. Modulation of nucleosomal DNA accessibility and ligase activity by histone acetylation. (*A*) Overview of nicked DNA-containing NCP reconstitution. Terminal 5′-phosphates in 601-DNA are removed by alkaline phosphatase treatment, followed by introduction of a single-strand nick by the site-specific endonuclease, Nt.BsmAI, 31 base pairs from the 3′ end of the sense strand. An AlexaFluor647 dye is added onto the 3′-end of the nicked strand before the DNA is incorporated into NCPs for ease of visualization in ligation assays (see *SI Appendix*, *Materials and Methods* for more details). (*B*) Denaturing gel images displaying the DNA products from ligation assays of NCPs with no acetylated histones ("unmodified") and NCPs containing acetylated H2A (remaining ligation assay gels are shown in *SI Appendix*, Fig. S10*A*). The position of the nicked fragment before ("Nicked") and after ligation is visualized by the fluorescence signal of the AlexaFluor647 dye adjoined to it. (*C*) Quantification of ligation in the unmodified NCPs, and NCPs containing mutant H2A (P116* and K73Q, K74Q, P116*). Solid lines are best fits from linear regression. (*D*) Rates of ligation of nicked nucleosomal DNA in NCPs with different combinations of acetylated histones, as indicated, given by the slopes of the linear fits in *C* and in *SI Appendix*, Fig. S10*B*. The error bars are errors of the slopes obtained from linear regression. (*Inset*) The position of the single-strand break is highlighted with a pink bolt. (*E*) Representative images of denaturing gels resolving the DNA degradation products from MNase digestion reactions containing the variably acetylated NCPs. DNA species are detected via SYBR Gold staining. Note that because the MNase assays were performed on nicked DNA samples, illustrated in *A*, three bands would be expected (see columns where MNase was not added) in the absence of any digestion, corresponding to a full-length 601-DNA strand (153 base pairs) and smaller fragments of 122 and 31 base pairs derived from the nicked strand.

stacking mode, as illustrated in the cryogenic electron micrograph of the unmodified sample showing extensive stacking of particles (Fig. 6 *B*, *Right Top*). The resulting dissociation constants for NCP addition ($K_D = 1/K_A$), R_h values, and slopes of R_h *vs* (NCP) profiles (Fig. 6*A*) are shown in Fig. 6*C*, and the distribution of particle sizes comprised of a given number of stacked NCPs is shown in *SI Appendix*, Fig. S11*B*.

Compared to unmodified particles, acetylation of single histones in the context of NCPs reduced the inter-NCP affinities regardless of which histone was modified, with a rank order of unmodified (strongest affinity) > AcH2A ~ AcH2B > AcH3 > AcH4. R_h values, extrapolated to zero NCP concentration ($R_{h,zero}$), also varied, with $R_{h,zero}$ values of the NCPs containing acetylated H2A or acetylated H3 being approximately 0.5 nm larger than for the other acetylated NCPs whose values were similar to the unmodified particle. Acetylation of H3, whose N-terminal tail is longest among the histones, may lead to an increase in effective particle size by extending the charge-neutralized large histone tail outward from the NCP. In the case of H2A, whose C-terminal tail interacts with the DNA entry/exit sites, the increased $R_{h,zero}$ may be the result of increasing nucleosomal DNA unwrapping, either by decreasing contacts directly with the acetylated tail, or perhaps indirectly, by weakening key H2A–DNA interactions involving, for example, K73 and K74 in the unmodified histone.

Discussion

Epigenetic modifications of chromatin add a critical layer to the regulation of gene activity (1, 2) and for controlling the fidelity of the genome (3, 5). An important marker is acetylation of lysine sidechains which modulates chromatin compaction (66) and hence transcription, regulates the phase separation propensity of chromatin (67), and serves as a signal for DNA damage repair (25). While it is known that epigenetic marks can affect the compaction level of chromatin, how marks on different histones, and at different sites within a given histone, result in site-specific motional changes over a range of time scales, and how such changes affect enzyme–nucleosomal DNA interactions remain largely unexplored. We have chosen to focus on each of the four core histones, one at a time, in the context of NCPs in much of

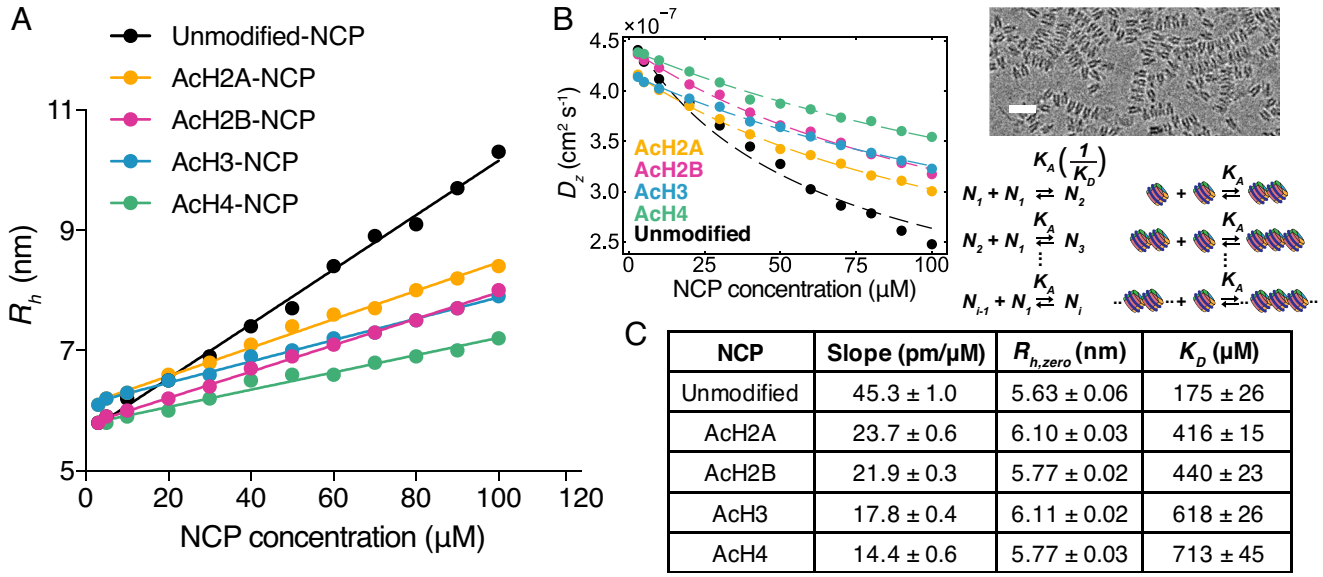

C

NCP	Slope (pm/μM)	$R_{h,zero}$ (nm)	K_D (μM)
Unmodified	45.3 ± 1.0	5.63 ± 0.06	175 ± 26
AcH2A	23.7 ± 0.6	6.10 ± 0.03	416 ± 15
AcH2B	21.9 ± 0.3	5.77 ± 0.02	440 ± 23
AcH3	17.8 ± 0.4	6.11 ± 0.02	618 ± 26
AcH4	14.4 ± 0.6	5.77 ± 0.03	713 ± 45

Fig. 6. Quantifying internucleosome interactions of unmodified and acetylated NCPs. (*A*) Hydrodynamic radii of NCPs plotted as a function of NCP concentration (AcH2A-NCP refers to an NCP with acetylated H2A and so forth). Hydrodynamic radii, R_h, were calculated using the Stokes–Einstein equation and diffusion constants from DLS shown in *B*. Solid lines are best fits from linear regression. (*B*) Diffusion constants of the unmodified and acetylated NCPs determined by DLS, 25 °C. Dashed lines are best fits obtained from the self-assembly model shown on the right side of the plot (*SI Appendix*), where it is assumed that NCPs stack on top of each other, as illustrated in the cryo-EM micrograph of unmodified NCPs, 100 mM NaCl, showing fiber-like structures. The white scale bar corresponds to 20 nm. (*C*) Parameters extracted from the fits in *A* and *B*.

this work, recognizing that despite their structural similarities, each histone plays distinct roles in maintaining and regulating nucleosome structure and dynamics. Further, our aim was to maximize the degree of acetylation on each histone, while still maintaining intact and well-formed particles (Fig. 1*A*), in order to amplify structural and motional changes and achieve as much sample homogeneity for NMR studies as possible. This approach comes with the cost of inaccurately recapitulating biological acetylation patterns. However, we believe that a more comprehensive degree of acetylation allowed us to uncover nuanced effects which may not have emerged if fewer sites were acetylated less regularly.

Here, focusing on NCPs as the simplest building block of chromatin, we have carried out backbone ^{15}N NMR spin relaxation experiments which establish that acetylation of a given histone has a marked effect on its tail dynamics, significantly increasing motion that results from a weakening of tail–DNA interactions. The magnitude of this effect varied among histones and was largest for H2A and H3, although within a given tail the motional changes did vary. In order to study the more ordered sections of the NCP, where ^{1}H–^{15}N NMR experiments fail, we have used methyl-TROSY-based approaches and highly deuterated, methyl protonated samples, again focusing on one histone at a time. A strong correlation of methyl group $S^2_{axis}\tau_C$ values for histones H2B, H3, and H4 with and without acetylation was observed, suggesting that there is little dynamic coupling between histone cores and tails on the ps-ns timescale, and that, therefore, the increased levels of tail motion resulting from acetylation is predominately a direct effect involving histone–DNA interactions. In contrast, acetylation of H2A had a significant effect on the structural dynamics of the core region of this histone, as evidenced by poor-quality ^{1}H–^{13}C correlation spectra (Fig. 3*A*), and significant changes in both ps-ns and μs-ms timescale motions (Fig. 4 *A* and C). Relaxation studies highlight that acetylation of H2A leads to significant changes in the dynamics of the docking domain and the L1 loop (see residues in Fig. 4 *B* and *C*, *Left*) that are integral to NCP stability, potentially contributing to the increased motion observed at the level of the H2A tails. Notably, the core H2A dynamics were largely suppressed in the (unacetylated) H2A P116* truncation mutant, suggesting that weakening of H2A tail–DNA interactions, either through acetylation of K117, K118, K121, and K122 or simply truncation of this region, is not sufficient to promote the conformational heterogeneity in the docking domain/L1 loop regions that was observed for highly acetylated H2A. Rather the conformational heterogeneity throughout the docking domain results from acetylation of lysine residues 73 and 74 in the L2 loop bridging helices α2 and α3, whose sidechains make direct electrostatic contacts with the DNA phosphate backbone in super helix location 6, since a mutant H2A (K73Q, K74Q, P116*) NCP construct was able to recapitulate these motions. We note that these lysine residues are known biological targets of acetylation (68), are mutated to Asn in H2A onco-histones (69), and are altered to Gly 78 and Glu 79 in human histone variant H2A.B (70). In a cryo-EM structure of NCPs containing H2A.B, these residue substitutions were associated with destabilization of the same DNA contacts described above (70), further pointing to the potential importance of K73 and K74 acetylation in regulating nucleosome structural dynamics in this region. In this regard, H2A.B-containing NCPs show an increase in accessibility to nucleases, increased propensity for DNA unwinding at the DNA exit/entry points, and decreases in the efficacy of chromatin remodeling by the chromatin structure remodeling complex (60).

In addition to the changes in dynamics of the docking domain that accompany acetylation of K73 and K74, it is likely that the corresponding modification of K35 increases conformational heterogeneity in the L1 loop, as probed by V42 that shows changes in μs-ms and ps-ns timescale dynamics (Fig. 4 *A* and *C*). The increased conformational heterogeneity in this region may be reporting on the destabilization of L1–L1 interactions that bridge the two H2A histones in the NCP, as acetylation of K35, located proximal to L1, would eliminate a salt-bridge linking this lysine to the DNA backbone (Fig. 4 *B*, *Right Bottom*). It may be that the unique proximity of this region to H2B could further implicate it in the cooperative effect we see with H2A-H2B acetylation in

the ligation assay (Fig. 5*D*). Such synergistic effects highlight the complexity by which acetylation regulates the structure and dynamics of the NCP to yield functional outcomes. Notably, H2A variants can differ significantly in amino acid composition from the canonical H2A in the L1 loop, thus regulating the structural dynamics in this region which then can propagate to more distal regions of the nucleosome (71). It seems likely that acetylation can achieve the same result.

The relaxation data presented here inform on intra-NCP interactions, as substantiated by several lines of evidence. First, by reducing the salt concentration by omitting sodium chloride from all NMR samples, as was done in this study, inter-NCP contacts are greatly attenuated. For example, although the effective sizes of particles (R_h) increase with NCP concentration in the presence of 100 mM salt (Fig. 6 *A* and *B*), a sign of interparticle interactions, the R_h vs. [NCP] profile without salt has the opposite slope (*SI Appendix*, Fig. S11*A*) resulting from nonideality effects associated with the charged NCPs (72). Second, although a very strong correlation between methyl group $S^2_{axis}\tau_C$ values is observed for histones H2B, H3, and H4 in acetylated and unmodified samples, the slight overall increase in $S^2_{axis}\tau_C$ upon acetylation, in particular for the H2B sample (Fig. 4*C*), argues against a contribution from inter-NCP contacts, as these are reduced upon acetylation (Fig. 6*A*) and would lead to a decrease in $S^2_{axis}\tau_C$. Rather, changes in $S^2_{axis}\tau_C$ point to an increase in particle size due to weakened contacts between histone tails and DNA that promotes an extension of the tails from the core. Third, a comparison of ps-ns timescale dynamics for H3 tails shows little difference between samples prepared in buffers with either 0 or 100 mM sodium chloride, consistent with little effect from association between particles (*SI Appendix*, Fig. S12). Acetylation does, however, have a pronounced role in regulating chromatin structure (i.e., decreasing inter-NCP interactions in chromatin (34, 73)), and the importance of the H4 tail in controlling compaction of chromatin through internucleosome contacts via the acidic patch has been well documented (65), especially in simulations (74) and through experiments involving polynucleosomal arrays (34, 73). Notably, we were able to recapitulate these effects with individual NCPs, showing that acetylation attenuates particle oligomerization in a histone-dependent manner, with acetylated H4 NCPs the most protective against aggregation. A simple oligomerization scheme was developed (Fig. 6*B* and *SI Appendix*, *Materials and Methods*) which explains NCP concentration-dependent DLS data recorded at 0.1 M NaCl, with acetylation of H4 decreasing inter-NCP association by a factor of three. Acetylation-dependent modulation of H4 tail interactions can cause even larger-scale perturbations involving internucleosomal interactions that regulate phase separation (67).

In summary, our results highlight the nuanced roles that histone acetylation plays in modulating nucleosome core particle structural dynamics. H2A, in particular, has been identified as containing hot spot regions where the dynamics are significantly affected by acetylation, leading to pronounced changes in interactions between NCPs and protein factors. In this regard, it is of interest to note that among the four histones, the H2A family is the most diverse (55, 60), with replacement of one H2A family member with another leading to changes in chromatin structure and function (55). In a similar manner, acetylation of H2A leads to changes in dynamics in regions that are least conserved in the H2A family, such as the docking domain and the L1 loop, providing yet another mechanism for modulating biological output.

Materials and Methods

All NMR experiments were recorded using either 14.1 T or 18.8 T Bruker Avance III HD spectrometers, or with a 23.5 T Bruker Avance NEO spectrometer, each equipped with an *x*, *y*, *z* gradient TCI cryoprobe. All experiments on NCP samples, at concentrations varying between ~90 μM and 110 μM, were recorded at 37 °C. Details of protein expression and purification, acetylation reactions, ligation and MNase assays, and NMR experiments are provided in *SI Appendix*.

Data, Materials, and Software Availability. All study data are included in the article and/or *SI Appendix*.

ACKNOWLEDGMENTS. We are grateful to Dr. Peter Schuck, NIH, Bethesda, MD, for discussions regarding nonideality of diffusing charged particles in solution and Professor Hyun Kate Lee, University of Toronto, for discussions on the biochemical assays. T.H.K. was supported by a Banting postdoctoral fellowship from the Canadian Institutes of Health Research (CIHR) and the H. L. Holmes Award from the National Research Council of Canada. M.L.N. acknowledges an Alexander Graham Bell Canada Graduate Doctoral Scholarship from the Natural Sciences and Engineering Research Council of Canada (NSERC). N.B.-C., R.W.H., and S.K.H. acknowledge postdoctoral support from the CIHR and the Hospital for Sick Children Research Institute (R.W.H). This research was funded by CIHR grant FDN-503573 (L.E.K.) and NSERC grant FDN-455908 (L.E.K.).

Author affiliations: [a]Department of Molecular Genetics, University of Toronto, Toronto, ON M5S 1A8, Canada; [b]Department of Biochemistry, University of Toronto, Toronto, ON M5S 1A8, Canada; [c]Department of Chemistry, University of Toronto, Toronto, ON M5S 1A8, Canada; and [d]Program in Molecular Medicine, Hospital for Sick Children, Toronto, ON M5G 1X8, Canada

1. A. J. Bannister, T. Kouzarides, Regulation of chromatin by histone modifications. *Cell Res.* **21**, 381–395 (2011).
2. E. R. Gibney, C. M. Nolan, Epigenetics and gene expression. *Heredity (Edinb)* **105**, 4–13 (2010).
3. A. Fernandez *et al.*, Epigenetic mechanisms in DNA double strand break repair: A clinical review. *Front. Mol. Biosci.* **8**, 685440 (2021).
4. A. K. Deem, X. Li, J. K. Tyler, Epigenetic regulation of genomic integrity. *Chromosoma* **121**, 131–151 (2012).
5. E. L. Putiri, K. D. Robertson, Epigenetic mechanisms and genome stability. *Clin. Epigenetics* **2**, 299–314 (2011).
6. Y. Atlasi, H. G. Stunnenberg, The interplay of epigenetic marks during stem cell differentiation and development. *Nat. Rev. Genet.* **18**, 643–658 (2017).
7. Z. Zhao, A. Shilatifard, Epigenetic modifications of histones in cancer. *Genome Biol.* **20**, 245 (2019).
8. F. Miao *et al.*, Evaluating the role of epigenetic histone modifications in the metabolic memory of type 1 diabetes. *Diabetes* **63**, 1748–1762 (2014).
9. A. Portela, M. Esteller, Epigenetic modifications and human disease. *Nat. Biotechnol.* **28**, 1057–1068 (2010).
10. Y. Zhao, B. A. Garcia, Comprehensive catalog of currently documented histone modifications. *Cold Spring Harb. Perspect. Biol.* **7**, a025064 (2015).
11. T. G. Gillette, J. A. Hill, Readers, writers, and erasers: Chromatin as the whiteboard of heart disease. *Circ. Res.* **116**, 1245–1253 (2015).
12. G. Smeenk, N. Mailand, Writers, readers, and erasers of histone ubiquitylation in DNA double-strand break repair. *Front. Genet.* **7**, 122 (2016).
13. K. Hyun, J. Jeon, K. Park, J. Kim, Writing, erasing and reading histone lysine methylations. *Exp. Mol. Med.* **49**, e324 (2017).
14. L. Verdone, E. Agricola, M. Caserta, E. di Mauro, Histone acetylation in gene regulation. *Brief. Funct. Genomic. Proteomic.* **5**, 209–221 (2006).
15. M. Grunstein, Histone acetylation in chromatin structure and transcription. *Nature* **389**, 349–352 (1997).
16. E. J. Richards, S. C. R. Elgin, Epigenetic codes for heterochromatin formation and silencing: Rounding up the usual suspects. *Cell* **108**, 489–500 (2002).
17. T. Narita *et al.*, Enhancers are activated by p300/CBP activity-dependent PIC assembly, RNAPII recruitment, and pause release. *Mol. Cell* **81**, 2166–2182.e6 (2021).
18. B. M. Dancy, P. A. Cole, Protein lysine acetylation by p300/CBP. *Chem. Rev.* **115**, 2419–2452 (2015).
19. R. L. Schiltz *et al.*, Overlapping but distinct patterns of histone acetylation by the human coactivators p300 and PCAF within nucleosomal substrates. *J. Biol. Chem.* **274**, 1189–1192 (1999).
20. C. Peña *et al.*, The expression levels of the transcriptional regulators p300 and CtBP modulate the correlations between SNAIL, ZEB1, E-cadherin and vitamin D receptor in human colon carcinomas. *Int. J. Cancer* **119**, 2098–2104 (2006).
21. R. H. Goodman, S. Smolik, CBP/p300 in cell growth, transformation, and development. *Genes Dev.* **14**, 1553–1577 (2000).

22. M. M. Vleugel, D. Shvarts, E. van der Wall, P. J. van Diest, p300 and p53 levels determine activation of HIF-1 downstream targets in invasive breast cancer. *Hum. Pathol.* **37**, 1085–1092 (2006).
23. D. Piekna-Przybylska, R. A. Bambara, L. Balakrishnan, Acetylation regulates DNA repair mechanisms in human cells. *Cell Cycle* **15**, 1506–1517 (2016).
24. S. Dhar, O. Gursoy-Yuzugullu, R. Parasuram, B. D. Price, The tale of a tail: Histone H4 acetylation and the repair of DNA breaks. *Philosophical Trans. R. Soc. B Biol. Sci.* **372**, 20160284 (2017).
25. C. R. Hunt *et al.*, Histone modifications and DNA double-strand break repair after exposure to ionizing radiations. *Radiat. Res.* **179**, 383–392 (2013).
26. D. R. Banerjee, C. E. Deckard, Y. Zeng, J. T. Sczepanski, Acetylation of the histone H3 tail domain regulates base excision repair on higher-order chromatin structures. *Sci. Rep.* **9**, 15972 (2019).
27. N. Horikoshi *et al.*, Pre-existing H4K16ac levels in euchromatin drive DNA repair by homologous recombination in S-phase. *Commun. Biol.* **2**, 253 (2019).
28. H. Ogiwara *et al.*, Histone acetylation by CBP and p300 at double-strand break sites facilitates SWI/SNF chromatin remodeling and the recruitment of non-homologous end joining factors. *Oncogene* **30**, 2135–2146 (2011).
29. A. T. Annunziato, J. C. Hansen, Role of histone acetylation in the assembly and modulation of chromatin structures. *Gene Expr.* **9**, 37–61 (2000).
30. V. Tugarinov, P. M. Hwang, J. E. Ollerenshaw, L. E. Kay, Cross-correlated relaxation enhanced 1H–13C NMR spectroscopy of methyl groups in very high molecular weight proteins and protein complexes. *J. Am. Chem. Soc.* **125**, 10420–10428 (2003).
31. H. Kato *et al.*, Architecture of the high mobility group nucleosomal protein 2-nucleosome complex as revealed by methyl-based NMR. *Proc. Natl. Acad. Sci. U.S.A.* **108**, 12283–12288 (2011).
32. G. Abramov, A. Velyvis, E. Rennella, L. E. Wong, L. E. Kay, A methyl-TROSY approach for NMR studies of high-molecular-weight DNA with application to the nucleosome core particle. *Proc. Natl. Acad. Sci. U.S.A.* **117**, 12836–12846 (2020).
33. E. A. Morrison, S. Bowerman, K. L. Sylvers, J. Wereszczynski, C. A. Musselman, The conformation of the histone H3 tail inhibits association of the BPTF PHD finger with the nucleosome. *Elife* **7**, e31481 (2018).
34. B.-R. Zhou *et al.*, Histone H4 K16Q mutation, an acetylation mimic, causes structural disorder of its N-terminal basic patch in the nucleosome. *J. Mol. Biol.* **421**, 30–37 (2012).
35. A. Furukawa *et al.*, Acetylated histone H4 tail enhances histone H3 tail acetylation by altering their mutual dynamics in the nucleosome. *Proc. Natl. Acad. Sci. U.S.A.* **117**, 19661–19663 (2020).
36. A. Stützer *et al.*, Modulations of DNA contacts by linker histones and post-translational modifications determine the mobility and modifiability of nucleosomal H3 tails. *Mol. Cell* **61**, 247–259 (2016).
37. M. Zandian *et al.*, Conformational dynamics of histone H3 tails in chromatin. *J. Phys. Chem. Lett.* **12**, 6174–6181 (2021).
38. G. A. Armeev, A. S. Kniazeva, G. A. Komarova, M. P. Kirpichnikov, A. K. Shaytan, Histone dynamics mediate DNA unwrapping and sliding in nucleosomes. *Nat. Commun.* **12**, 2387 (2021).
39. Y. Peng, S. Li, A. Onufriev, D. Landsman, A. R. Panchenko, Binding of regulatory proteins to nucleosomes is modulated by dynamic histone tails. *Nat. Commun.* **12**, 5280 (2021).
40. S. Schütz, R. Sprangers, Methyl TROSY spectroscopy: A versatile NMR approach to study challenging biological systems. *Prog. Nucl. Magn Reson Spectrosc* **116**, 56–84 (2020).
41. G. Ortega, M. Pons, O. Millet, "Chapter Six - Protein functional dynamics in multiple timescales as studied by NMR spectroscopy" in *Advances in Protein Chemistry and Structural Biology*, T. Karabencheva-Christova, Ed. (Academic Press, 2013), pp. 219–251.
42. M. Shogren-Knaak *et al.*, Histone H4–K16 acetylation controls chromatin structure and protein interactions. *Science* **311**, 844–847 (2006).
43. P. T. Lowary, J. Widom, New DNA sequence rules for high affinity binding to histone octamer and sequence-directed nucleosome positioning. *J. Mol. Biol.* **276**, 19–42 (1998).
44. H. Kato, J. Gruschus, R. Ghirlando, N. Tjandra, Y. Bai, Characterization of the N-terminal tail domain of histone H3 in condensed nucleosome arrays by hydrogen exchange and NMR. *J. Am. Chem. Soc.* **131**, 15104–15105 (2009).
45. V. Tugarinov, L. E. Kay, An isotope labeling strategy for methyl TROSY spectroscopy. *J. Biomol. NMR* **28**, 165–172 (2004).
46. S. Grzesiek, J. Anglister, A. Bax, Correlation of backbone amide and aliphatic side-chain resonances in 13C/15N-enriched proteins by isotropic mixing of 13C magnetization. *J. Magn. Reson. B* **101**, 114–119 (1993).
47. M. Ikura, L. E. Kay, A. Bax, A novel approach for sequential assignment of proton, carbon-13, and nitrogen-15 spectra of larger proteins: Heteronuclear triple-resonance three-dimensional NMR spectroscopy. Application to calmodulin. *Biochemistry* **29**, 4659–4667 (1990).
48. A. C. Conibear, K. J. Rosengren, C. F. W. Becker, H. Kaehlig, Random coil shifts of posttranslationally modified amino acids. *J. Biomol. NMR* **73**, 587–599 (2019).
49. C. L. van Emmerik, H. van Ingen, Unspinning chromatin: Revealing the dynamic nucleosome landscape by NMR. *Prog. Nucl. Magn. Reson. Spectrosc.* **110**, 1–19 (2019).
50. D. F. Hansen *et al.*, An exchange-free measure of 15N transverse relaxation: An NMR spectroscopy application to the study of a folding intermediate with pervasive chemical exchange. *J. Am. Chem. Soc.* **129**, 11468–11479 (2007).
51. J. Ausio, K. E. van Holde, Histone hyperacetylation: Its effects on nucleosome conformation and stability. *Biochemistry* **25**, 1421–1428 (1986).
52. R. T. Simpson, Structure of chromatin containing extensively acetylated H3 and H4. *Cell* **13**, 691–699 (1978).
53. D. F. Hansen, H. Feng, Z. Zhou, Y. Bai, L. E. Kay, Selective characterization of microsecond motions in proteins by NMR relaxation. *J. Am. Chem. Soc.* **131**, 16257–16265 (2009).
54. D. M. Korzhnev, K. Kloiber, V. Kanelis, V. Tugarinov, L. E. Kay, Probing slow dynamics in high molecular weight proteins by methyl-TROSY NMR spectroscopy: Application to a 723-residue enzyme. *J. Am. Chem. Soc.* **126**, 3964–3973 (2004).
55. C. Bönisch, S. B. Hake, Histone H2A variants in nucleosomes and chromatin: More or less stable? *Nucleic Acids Res.* **40**, 10719–10741 (2012).
56. J. Tazi, A. Bird, Alternative chromatin structure at CpG islands. *Cell* **60**, 909–920 (1990).
57. T. R. Hebbes, A. L. Clayton, A. W. Thorne, C. Crane-Robinson, Core histone hyperacetylation co-maps with generalized DNase I sensitivity in the chicken beta-globin chromosomal domain. *EMBO J.* **13**, 1823–1830 (1994).
58. E. Cotner-Gohara *et al.*, Human DNA ligase III recognizes DNA ends by dynamic switching between two DNA-bound states. *Biochemistry* **49**, 6165–6176 (2010).
59. I. D. Odell *et al.*, Nucleosome disruption by DNA ligase III-XRCC1 promotes efficient base excision pepair. *Mol. Cell Biol.* **31**, 4623–4632 (2011).
60. M. S. Shukla *et al.*, The docking domain of histone H2A is required for H1 binding and RSC-mediated nucleosome remodeling. *Nucleic Acids Res.* **39**, 2559–2570 (2011).
61. M. A. Keene, S. C. R. Elgin, Micrococcal nuclease as a probe of DNA sequence organization and chromatin structure. *Cell* **27**, 57–64 (1981).
62. C. M. Rivera, B. Ren, Mapping human epigenomes. *Cell* **155**, 39–55 (2013).
63. T. Schalch, S. Duda, D. F. Sargent, T. J. Richmond, X-ray structure of a tetranucleosome and its implications for the chromatin fibre. *Nature* **436**, 138–141 (2005).
64. F. Gordon, K. Luger, J. C. Hansen, The core histone N-terminal tail domains function independently and additively during salt-dependent oligomerization of nucleosomal arrays. *J. Biol. Chem.* **280**, 33701–33706 (2005).
65. P.-Y. Kan, T. L. Caterino, J. J. Hayes, The H4 tail domain participates in intra- and internucleosome interactions with protein and DNA during folding and oligomerization of nucleosome arrays. *Mol. Cell Biol.* **29**, 538–546 (2009).
66. M. Shogren-Knaak *et al.*, Histone H4–K16 acetylation controls chromatin structure and protein interactions. *Science* **311**, 844–847 (2006).
67. B. A. Gibson *et al.*, Organization of chromatin by intrinsic and regulated phase separation. *Cell* **179**, 470–484.e21 (2019).
68. D. Li *et al.*, Identification of histone acetylation markers in human fetal brains and increased H4K5ac expression in neural tube defects. *Mol. Genet. Genomic. Med.* **7**, e1002 (2019).
69. B. A. Nacev *et al.*, The expanding landscape of 'oncohistone' mutations in human cancers. *Nature* **567**, 473–478 (2019).
70. M. Zhou *et al.*, Structural basis of nucleosome dynamics modulation by histone variants H2A.B and H2A.Z.2.2. *EMBO J.* **40**, e105907 (2021).
71. S. Bowerman, J. Wereszczynski, Effects of macroH2A and H2A.Z on nucleosome dynamics as elucidated by molecular dynamics simulations. *Biophys. J.* **110**, 327–337 (2016).
72. K. S. Schmitz, "Polyelectrolyte solutions" in *Introduction to Dynamic Light Scattering by Macromolecules* (Elsevier, 1990), pp. 205–259.
73. A. Allahverdi *et al.*, The effects of histone H4 tail acetylations on cation-induced chromatin folding and self-association. *Nucleic Acids Res.* **39**, 1680–1691 (2011).
74. R. Zhang, J. Erler, J. Langowski, Histone acetylation regulates chromatin accessibility: Role of H4K16 in inter-nucleosome interaction. *Biophys. J.* **112**, 450–459 (2017).